


RESEARCH

Open Access



Effects and mechanisms of breastmilk stem cells in the treatment of white matter injury in newborn rats

Meng Zhang^{1,2†}, Haoran Wang^{2†}, Yang He^{1,2}, Wenxing Li^{1,2}, Hongju Chen^{1,2}, Xinyu Zhang^{1,2}, Qiang Chen³, Chao Yang³, Maowen Luo³, Bo Zhang³, Jun Tang^{1*}  and Dezhi Mu^{1,2*}

Abstract

Background Breastmilk stem cells (BSCs) have been reported to have potential benefits for infants. However, whether the BSCs could improve brain injury is unknown. A culture system for BSCs was established, and the roles of BSCs in treating white matter injury (WMI) were investigated in our study.

Methods Breastmilk samples were collected from healthy lactating women between days 1 and 5 after delivery. The BSCs were cultured in a specialized culture medium and then characterized through flow cytometry and immunofluorescence methods. A rat model with WMI was established by ligating the right carotid artery of Sprague–Dawley rats at postnatal day 3 (P3) and exposing the rats to 6% hypoxia for 2 h. Rats were categorized into sham, WMI with breastmilk cell (WMI + BC), and WMI with (WMI + NS) groups. In the WMI + BC group, 5 μ L BCs (1×10^6) was injected into the lateral ventricle 24 h post-modeling. Four different stages of oligodendrocyte (OL) markers were observed. Long-term neurobehavioral evaluations were conducted using the Morris water maze test. The inflammatory cytokines and proportion of proinflammatory microglial cells were detected to study the mechanisms of BSC treatment.

Results The isolated BSCs expressed mesenchymal stem cell-positive markers, including *CD105*, *CD73*, *CD29*, *CD166*, *CD44*, and *CD90*. Meanwhile, the mesenchymal stem cell-negative markers, including *HLA-DR*, *CD45*, and *CD79a*, were also found in BSCs. The BSCs did not express pluripotent stem cell markers, including *SOX2*, *Nanog*, *OCT4*, *SSEA4*, and *TRA-1-60*. Immunofluorescence detection showed that BSCs expressed neural stem/progenitor cell markers, including *Vimentin*, *Nestin*, and *A2B5*. Following BSC treatment, pathological improvements were observed in WMI. The expressions of mature OLs markers myelin basic protein and myelin-associated glycoprotein were increased in the corpus callosum and periventricular areas. Meanwhile, the numbers of myelin sheath increased, and learning and memory abilities improved. Furthermore, a decrease in *B7-2*/*Iba1* + proinflammatory microglia and an increase in

[†]Meng Zhang and Haoran Wang contributed equally to this work.

*Correspondence:

Jun Tang
tj1234753@sina.com
Dezhi Mu
mudz@scu.edu.cn

Full list of author information is available at the end of the article



© The Author(s) 2025. **Open Access** This article is licensed under a Creative Commons Attribution-NonCommercial-NoDerivatives 4.0 International License, which permits any non-commercial use, sharing, distribution and reproduction in any medium or format, as long as you give appropriate credit to the original author(s) and the source, provide a link to the Creative Commons licence, and indicate if you modified the licensed material. You do not have permission under this licence to share adapted material derived from this article or parts of it. The images or other third party material in this article are included in the article's Creative Commons licence, unless indicated otherwise in a credit line to the material. If material is not included in the article's Creative Commons licence and your intended use is not permitted by statutory regulation or exceeds the permitted use, you will need to obtain permission directly from the copyright holder. To view a copy of this licence, visit <http://creativecommons.org/licenses/by-nc-nd/4.0/>.

CD206+/Iba1 + anti-inflammatory microglia were observed. The mRNA expressions of proinflammatory factors (*Il1b*, *Il6*, *Ifng*, and *Tnfa*) and anti-inflammatory factors (*Arg1* and *Tgfb*) decreased and increased, respectively.

Conclusion Our findings suggest that BSCs can improve the maturation of OLs following WMI in newborn rats. The mechanisms may be attributed to the reduced proinflammatory microglia cells and factors as well as the increased anti-inflammatory microglia cells and factors.

Keywords Preterm infants, White matter injury, Breastmilk stem cells, Oligodendrocyte differentiation and maturation, Neuroinflammation

Background

White matter injury (WMI) is the predominant type of brain injury among preterm infants. Approximately 5–15% of very preterm infants develop severe neurological sequelae, whereas 25–50% experience mild cognitive impairments, learning difficulties, and behavioral conditions [1]. Such brain injuries significantly harm the physical and mental well-being of children and impose an economic burden on families and society. Oligodendrocyte (OL) differentiation and myelination disorders are the main pathological changes in WMI. The pathogenesis of WMI involves neuroinflammation, cell death, oxidative stress, and generation of free radicals [2]. Symptomatic supportive treatment is typically used for WMI [3]. WMI is a transient, nonprogressive condition, and the low immunogenicity environment of the brain makes it more conducive for cell transplantation therapy. Recent studies have shown that stem cells provide a new therapeutic option for addressing WMI [4].

Breastfeeding confers numerous benefits to infants, spanning growth, immunity, and societal and psychological aspects, among others [5]. Breastmilk stem cells (BSCs) were first identified in 2007. Nestin-positive cells were found in breastmilk, suggesting the potential existence of pluripotent stem cells [6]. Subsequent research revealed that BSCs exhibit mesenchymal properties and can differentiate into cell lineages of fat, cartilage, and bone [7]. However, other studies have suggested that the genes expressed by BSCs are similar to those expressed by human embryonic stem cells [8]. Discrepancies in the cellular properties of BSCs across different studies may stem from variations in medium composition, culture methods, and breastmilk collection techniques. A notable advantage of BSCs lies in their noninvasive acquisition, which offers broad application prospects.

Therefore, we aimed to establish a culture system for BSCs, isolate and culture them, and identify their surface markers. We also developed a neonatal WMI model in postnatal day 3 (P3) Sprague–Dawley (SD) rats to investigate the safety, effectiveness, and underlying mechanisms of BSCs in treating neonatal WMI.

Methods

Collection of breastmilk samples

This study was approved by the Institutional Ethics Committee of West China Second Hospital, Sichuan University (no. 2020083). Breastmilk samples were obtained from healthy lactating women from postpartum days 1 and 5. Before enrollment, participants were briefed on the study's methods and objectives, and their informed written consent was obtained. Colostrum samples (5–50 mL) were collected in sterile 15-mL centrifuge tubes containing antibiotics (1–2 mL penicillin–streptomycin) using sterile procedures.

Isolation and culture of breastmilk cells

Equal volumes of sterile normal saline (NS) were used to dilute the breastmilk, and the solution was centrifuged at $810 \times g$ for 20 min at 4°C. The skim milk liquid and fat layers were then removed. Subsequently, 10 mL sterile NS was added to the remaining cell pellet, and the solution was centrifuged for 5 min at 4°C at $710 \times g$. After centrifugation, the liquid component was discarded, and the procedure was repeated at $500 \times g$ for 5 min at 4°C. The pellet was then suspended in 1 mL culture medium (Supplementary Table 1), counted, and inoculated into a T25 cell culture flask at a $0.5\text{--}1 \times 10^6/\text{cm}^2$ density. The culture medium in each flask was supplemented to 3–5 mL, and the cells were incubated at 5% CO₂ and 37°C. The culture medium was changed daily for the first 5 days, after which, it was changed every 3 days.

Collection of BSCs

Primary cultured cells were observed under a microscope every 3 days. When the cells reached approximately 70–90% confluency, the primary culture cells in each bottle were washed with 5 mL NS two to three times after removing the culture medium. Subsequently, 0.5 mL 0.25% trypsin was added for digestion (approximately 5 min at 37°C). Next, 5 mL culture medium was added to the culture bottle, and the cell pellet was resuspended using a pipette. Centrifugation was repeated, and the cell pellets were collected.

Flow cytometry and Immunofluorescence for BSCs

Mesenchymal and embryonic stem cell markers, including *CD90*, *CD105*, *CD45*, *CD34*, *CD73*, *CD29*, *CD79a*, *CD44*, *CD166*, *CD11a/CD18*, *STRO-1*, *SOX2*, *OCT4*, *TRA-1-60*, *SSEA4*, and *Nanog*, were used to characterize BSCs through flow cytometry. The BSC culture was incubated in a dark room for 20 min at room temperature, centrifuged at $500 \times g$ for 5 min, and resuspended with 300 μ L phosphate-buffered saline (PBS).

Through the immunofluorescence method, antibodies such as *Vimentin*, *Nestin*, *A2B5*, *SOX2*, *OCT4*, *TRA-1-60*, and *SSEA4* were used to characterize the BSCs using neural stem/progenitor cells and embryonic stem cell markers. Initially, the cultured cells were rinsed with PBS three times. Subsequently, the cells were fixed with 4% paraformaldehyde at 4 °C for 20 min. After washing with PBS, the cells were incubated in PBS containing 0.3% Triton at room temperature for 30 min. Following three additional washes with PBS, the cells were kept in PBS containing 4% goat serum at room temperature for 1 h. Antibodies were diluted in PBS containing 0.3% Triton, 2% goat serum, and 3% serum albumin. Diluted antibodies were added to the BSCs, and the samples were incubated at room temperature overnight. Subsequently, the cells were washed three times with PBS. Secondary antibodies and 4',6-diamidino-2-phenylindole (DAPI) were added, and the samples were incubated for 2 h at room temperature. Finally, the cells were observed under a fluorescence microscope.

Establishment of the WMI model in neonatal rats

P3 SD rats (specific pathogen-free grade) were purchased from Chengdu Dashuo Medical Experimental Animal Co., Ltd. The animal room was set on a 12-hour light/12-hour darkness cycle. The surgery was conducted with continuous inhalation of isoflurane to maintain anesthesia. The skin and subcutaneous tissue of the neck were systematically separated from the right side of the adjacent trachea layer by layer, and the right common carotid artery was identified. After carefully dissecting the artery and vagus nerve, the right carotid artery was ligated and severed. Rats in the WMI group were allowed a 1-h rest period in their cages following surgical treatment. Then, they were placed in a 6% oxygen + 94% nitrogen oxygen deficiency chamber for 2 h of hypoxia treatment. The WMI model was identified using laser speckle cerebral blood flow imaging, hematoxylin and eosin (H&E) staining, immunofluorescence, and the Morris water maze (MWM) test.

Intraventricular injection of BSCs

Intraventricular injection was administered 24 h post-modeling. Rats were isoflurane anesthetized (R510-22-10; RWD), and 5 μ L cells or NS were stereotactically injected

into the ipsilateral hemisphere intraventricularly at a flow rate of 1 μ L/min. The injection site was positioned 2 mm posterior and 2 mm lateral to the bregma and 3 mm below the skull surface. Rats were randomly categorized into WMI + BC (breastmilk cells), WMI + NS, and sham groups. In the WMI + BC group, 1×10^6 BCs (5 μ L) were injected into the lateral ventricle 24 h post-modeling. In the WMI + NS group, 5 μ L NS was injected. In the sham group, only the right carotid artery was separated. Rats were euthanized by cervical dislocation following isoflurane anesthesia (R510-22-10; RWD). Subsequently, their organs were collected for further experiments.

Migration and differentiation of BSCs after injection

BSCs were labeled with PKH26 following the manufacturer's instructions. Briefly, 2×10^7 BSCs were washed and centrifuged at $400 \times g$ for 5 min. After discarding the supernatant, the cells were resuspended and fully dissolved in 1 mL Solution C. PKH26 staining reagent (4 μ L diluted in 1 mL Solution C) was prepared before labeling. The cells were immediately mixed with the PKH26 reagent and incubated at 25 °C for 5 min, followed by gentle mixing. Staining was halted by adding an equal volume of serum for a 1-min incubation period. Subsequently, the cells were centrifuged at $400 \times g$ for 10 min at 25 °C. The supernatant was removed, and the cells were resuspended in NS. The differentiation of BSCs in the rat brain was assessed using immunofluorescence 7 days post-transplantation to observe whether PKH26 was co-stained with nerve cell markers (NeuN and Olig2).

Immunofluorescence

Immunofluorescence was conducted using brain tissue collected at P7 and P14. The brain tissue was fixed in 4% paraformaldehyde and then embedded in an optimal cutting temperature compound at -80 °C for at least 2 h. Coronal Sect. (12 μ m) of the embedded brain tissue, focusing on the corpus callosum (CC), were obtained using a microtome cryostat (Leica). For immunofluorescence labeling, the sections were blocked with PBS, 0.5% serum, and 0.3% Triton X-100 for 1 h. Subsequently, the sections were incubated overnight at 4 °C in the following primary antibody solutions: mouse anti-myelin basic protein (anti-MBP) (1:500; Millipore), mouse anti-myelin-associated glycoprotein (anti-MAG) (1:500; Millipore), rabbit anti-NG2 (1:200, ab129051; Abcam), mouse anti-O4 immunoglobulin (Ig) M (1:25, MAB345; Millipore), and mouse anti-Olig2 (1:200, MABN50; Millipore). After washing, the sections were incubated with secondary antibodies (488-conjugated donkey anti-rabbit IgG and 488-conjugated donkey anti-mouse IgG, 1:500; Jackson ImmunoResearch) at room temperature for 2 h. Nuclei were counterstained with DAPI (1:500; Sigma Aldrich). Then, brain fluorescence imaging was

conducted and analyzed using a digital slicing scanner (Pannoramic MIDI II). Mean fluorescence intensity was measured using ImageJ software.

H&E staining

Rats in each group were killed and perfused with NS and 4% paraformaldehyde through the left ventricle following chest opening. The brains were fixed in 4% formaldehyde for a minimum of 24 h and subsequently embedded in paraffin. The paraffin-embedded brains underwent treatment with xylene, dehydration through alcohol and distilled water gradient, coronal sectioning, and H&E staining. Pathological changes in brain tissues were then observed under a microscope.

Western blot

Protein concentrations in the CC tissues collected at P14 were assessed using a BCA protein assay kit (Pierce; Thermo Fisher Scientific). Samples were separated through sodium dodecyl sulfate–polyacrylamide gel electrophoresis and transferred onto nitrocellulose membranes (Thermo Fisher Scientific). Following blocking with 5% bovine serum albumin (Sigma-Aldrich) in Tris-buffered saline, membranes were incubated overnight at 4 °C with the following primary antibodies: anti-MBP (1:3000, MBP101; Millipore), anti-MAG (1:3000, MBP101; Millipore), anti-fractalkine (1:3000, ab25088; Abcam), anti-CX3CR1 (1:1000, 14-6093-81; Invitrogen), anti-B7-2 (1:3000, MA5-32078; Invitrogen), or anti- β -actin (1:5000, sc-2357; Santa Cruz Biotechnology). Horseradish peroxidase-coupled goat anti-mouse or anti-rabbit IgG (1:5000; GE Healthcare Life Science antibody) was used as the secondary antibody and incubated with the membranes for 1 h at room temperature. Binding signals were detected using a bioimaging system (Chem-Doc XRS+; Bio-Rad), and intensities were analyzed using ImageJ software.

Electron microscopy

On P28, brain tissues from the right CC were dissected (1 mm [3]) and immediately fixed in 2% glutaraldehyde. Following fixation in 1% osmium acid, the brain tissues were dehydrated in an acetone gradient ranging from 30 to 100%. The dehydrated tissues were embedded in epoxy resin and cut into 50-nm sections. These sections were then collected using a copper mesh and stained with uranyl acetate before being observed under a transmission electron microscope.

MWM test

The MWM test was conducted on P28 rats ($n=15$ per group) for 7 days. This included the first 6 days of the positioning navigation test and day 7 of the space exploration test. The MWM test was performed with video

tracking software (RWD China) using an overhead video camera system to automate behavioral testing and provide unbiased data analyses. For the equipment preparation, a circular black pool with a diameter of 150 cm and a depth of 50 cm was used. The pool was divided into four quadrants and filled with water maintained at 22 °C. High-contrast cues were positioned inside the pool above the water surface, and a 10-cm diameter black platform was submerged 1 cm below the water surface. For the positioning navigation test, each rat underwent four daily trials in different quadrants for 6 days. Each trial allowed the rat 90 s to locate the hidden platform, and the time taken to locate the platform was recorded. If a rat failed to reach the platform within 90 s, it was guided to the platform. Subsequently, the rats were allowed to spend 10 s on the platform to learn and memorize the cues. For the space exploration test, the platform was removed on day 7, and the rats were allowed to swim freely for 60 s. The time taken for a rat to cross the location of the removed platform was recorded.

Cytokine antibody assay

Antibody arrays (RayBio GSR-CAA-67 Rat 67 Cytokine Antibody Assay; Ray Biotech, Inc.) were used to identify cytokines potentially involved in BSC treatment. CC tissues from rats were collected at P7, and experimental procedures and analyses were conducted following the manufacturer's instructions. The fluorescence readout was detected using a laser fluorescence scanning system.

Real-time reverse transcription polymerase chain reaction

Gene expression in brain CC tissue was quantified using a real-time reverse transcription–polymerase chain reaction (RT-PCR). Total RNA was isolated using TRIzol reagent (Ambion, and mRNA was reverse-transcribed to cDNA using the RevertAid First Strand cDNA Synthesis Kit. qRT-PCR amplification of cDNA was conducted using an iTaq SYBR Green Supermix kit (Bio-Rad) in a CFX96™ real-time PCR system (BioRad). The Ct ($2\Delta\Delta C_t$) method was used to determine the relative expression of each gene, with the target gene expression normalized to that of *GAPDH*. The specific primers used in this qPCR analysis are listed in Supplementary Table 2.

Statistical analyses

A total of 190 rats were randomized into the study, of which 13 were excluded owing to severe low body weight, severe wound infection, or death from bleeding or unknown causes. In the study, n refers to the number of animals; all experiments were conducted in triplicate. Sample size was determined based on previous literature and experience. One-way analysis of variance was used to compare experimental data among animals in the sham, WMI+NS, and WMI+BC groups.

Student–Newman–Keuls or Dunnett’s tests were used for multiple comparisons. Continuous variables were presented as means with 95% confidence intervals, and differences between groups were considered significant if p -values were <0.05 . Experimental data were analyzed and reported using GraphPad Prism® version 7.0 (GraphPad Software). The work has been reported in line with the ARRIVE guidelines 2.0.

Results

Culture and identification of BSCs

The cells adhered to the wall after 3 days in the experimental medium. Clonal aggregation became noticeable after 6 days of culture, with the clones’ number and diameter significantly increasing by day 9 (Fig. 1A). Flow cytometry analysis revealed that breastmilk cells expressed *CD105*, *CD73*, *CD29*, *CD166*, *CD44*, and *CD90*. The mesenchymal stem cell–negative markers *HLA-DR*, *CD45*, and *CD79a* were also expressed (Fig. 1B). Also, the results of immunofluorescence found that the BSCs expressed *CD105* and *CD90*, while did not express *CD34* (Supplementary Fig. 1). Pluripotent stem cell markers, including *SOX2*, *Nanog*, *OCT4*, *SSEA4*, and *TRA-1-60*, were not detected in BSCs through flow cytometry (Fig. 1C). Similarly, immunofluorescence results revealed the absence of pluripotent stem cell markers (*SOX2*, *OCT4*, and *SSEA4*) in BSCs (Fig. 1D) while exhibiting expression of the neural stem/progenitor cell markers *Vimentin*, *Nestin*, *A2B5*, *CD133* and *Pax6* (Fig. 1E and Supplementary Fig. 2).

Hypoxic ischemia–induced WMI in neonatal rats

In the WMI group, the cerebral blood flow on the right side (carotid ligation side) was significantly lower than that on the other side (Fig. 2A). The right/left cerebral blood flow ratio within the region of interest in the WMI group was significantly decreased ($p < 0.05$). H&E staining revealed tightly arranged white matter tissue in the sham group, whereas in the WMI group, the white matter tissue appeared swollen and broken, exhibiting a disordered arrangement, loose structure, and widened gaps (Fig. 2B). Following WMI, a significant decrease ($p < 0.01$) was noted in the mean fluorescence intensities of MBP and MAG in the white matter of the CC area at P14 (Fig. 2C). Transmission electron microscopy demonstrated a significant reduction ($p < 0.01$) in myelin content in the WMI group accompanied by an irregular morphology (Fig. 2D). The MWM experiment results indicated a significant increase in escape latency among rats in the WMI group, alongside a notable decrease in the frequency of platform crossings and average residence time in the platform area (Fig. 2E).

Migration and differentiation of BSCs after injection

The locations of PKH26-labeled BSCs were observed at 12, 24, 48, and 72 h post-injection. At 12 h post-injection, concentrated red fluorescence was observed in the lateral ventricle, indicating no significant migration of the BSCs. However, from 24 to 72 h post-injection, a scattered red fluorescence distribution was noted in the CC region on the injured side (Fig. 3B). To investigate the potential differentiation and neurosubstitution role of BSCs post-injection, co-staining of PKH26 with an OL marker (*Olig2*) and a neuronal marker (*NeuN*) was observed 3 and 7 days post-injection. However, no co-staining cells of PKH26 with *Olig2* or *NeuN* were observed (Fig. 3C). The results indicate that BSCs failed to differentiate into OLs or neurons in the rat brain at 3 and 7 days post-injection.

Efficacy and safety of BSC injections after WMI

Figure 4A illustrates a schematic diagram detailing the establishment of the WMI model, treatment, and evaluation timeline. Compared with the WMI+NS group, the WMI+BC group showed significantly improved pathological changes in the white matter area of the injured side in newborn rats, leading to reduced swelling and breakage of nerve cells at P7 and P14 (Fig. 4B). Furthermore, in the MWM test, the WMI+BC group exhibited a shorter latency escape time and increased number and times of platform crossing at P28 ($p < 0.01$, Fig. 4D).

Liver function was evaluated using alanine transaminase and alkaline phosphatase. Renal function was evaluated using blood urea nitrogen levels at P7. No significant differences in liver and kidney functions were observed among the three groups. H&E staining of liver samples depicted a regular arrangement of liver cells with normal shapes across all groups. Similarly, renal H&E staining illustrated a clear renal tissue structure, normal glomerular shape, and normal renal tubule shape in the medulla, with no signs of tubular wall thickening or cell swelling (Fig. 4C).

Compared with the WMI+NS group, the WMI+BC group revealed a decreased expression of the pre-OL markers *NG2* and *O4* ($p < 0.01$, Fig. 5A) at P7 and an increased expression of the mature OL markers *MBP* and *MAG* ($p < 0.01$, Fig. 5B) at P14. Western blot analysis further confirmed the elevated *MBP* and *MAG* expression levels in the WMI+BC group compared with the WMI+NS group ($p < 0.01$, Fig. 5C and D) at P14. Full-length blots are presented in Supplementary Figs. 3 and 4. Moreover, transmission electron microscopy demonstrated that the WMI+BC group exhibited more myelination with a more regular pattern than the WMI+NS group at P14 ($p < 0.01$, Figure E).

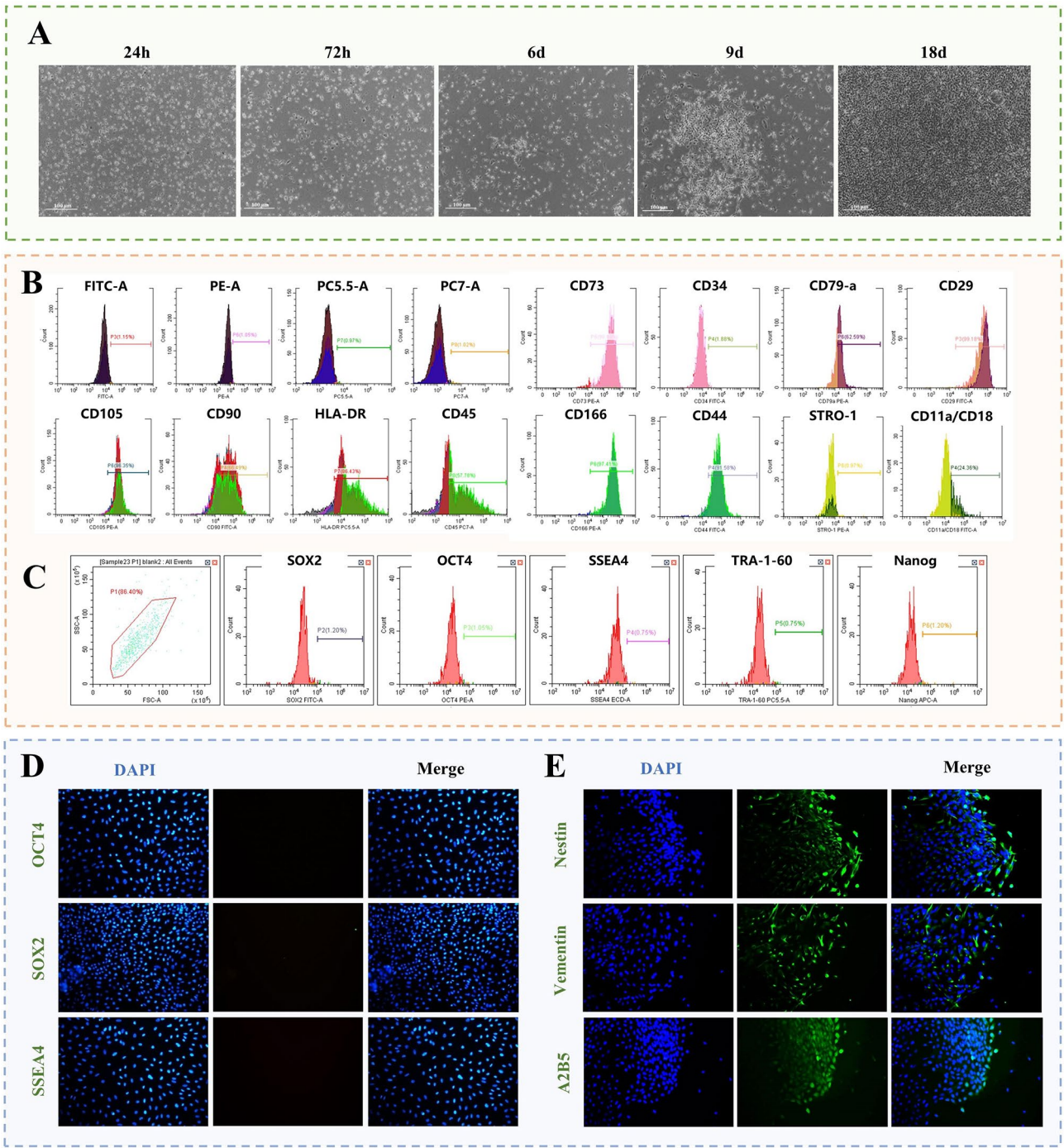


Fig. 1 Culture and identification of BSCs. **(A)** The proliferation and morphology of BSCs clones observed by microscope. Clonal aggregation became noticeable after 6 days of culture, with the clones' number and diameter significantly increasing by day 9. **(B)** Detection of mesenchymal stem cell markers via flow cytometry. The BSCs expressed the mesenchymal stem cell–positive markers *CD105*, *CD73*, *CD29*, *CD166*, *CD44*, and *CD90* and the mesenchymal stem cell–negative markers *HLA-DR*, *CD45*, and *CD79a*. **(C)** Detection of embryonic stem cell markers via flow cytometry. The BSCs did not express pluripotent stem cell markers, including *SOX2*, *Nanog*, *OCT4*, *SSEA4*, and *TRA-1-60*. **(D)** Immunofluorescence of embryonic stem cell markers (green). Nuclei were stained with DAPI (blue). The BSCs did not express pluripotent stem cell markers, including *SOX2*, *OCT4*, and *SSEA4*. **(E)** Immunofluorescence of neural stem/progenitor cell markers (green). Nuclei were stained with DAPI (blue). The BSCs expressed the neural stem/progenitor cell markers *Vimentin*, *Nestin*, and *A2B5*. BSCs, breastmilk stem cells; DAPI, 4',6-diamidino-2-phenylindole

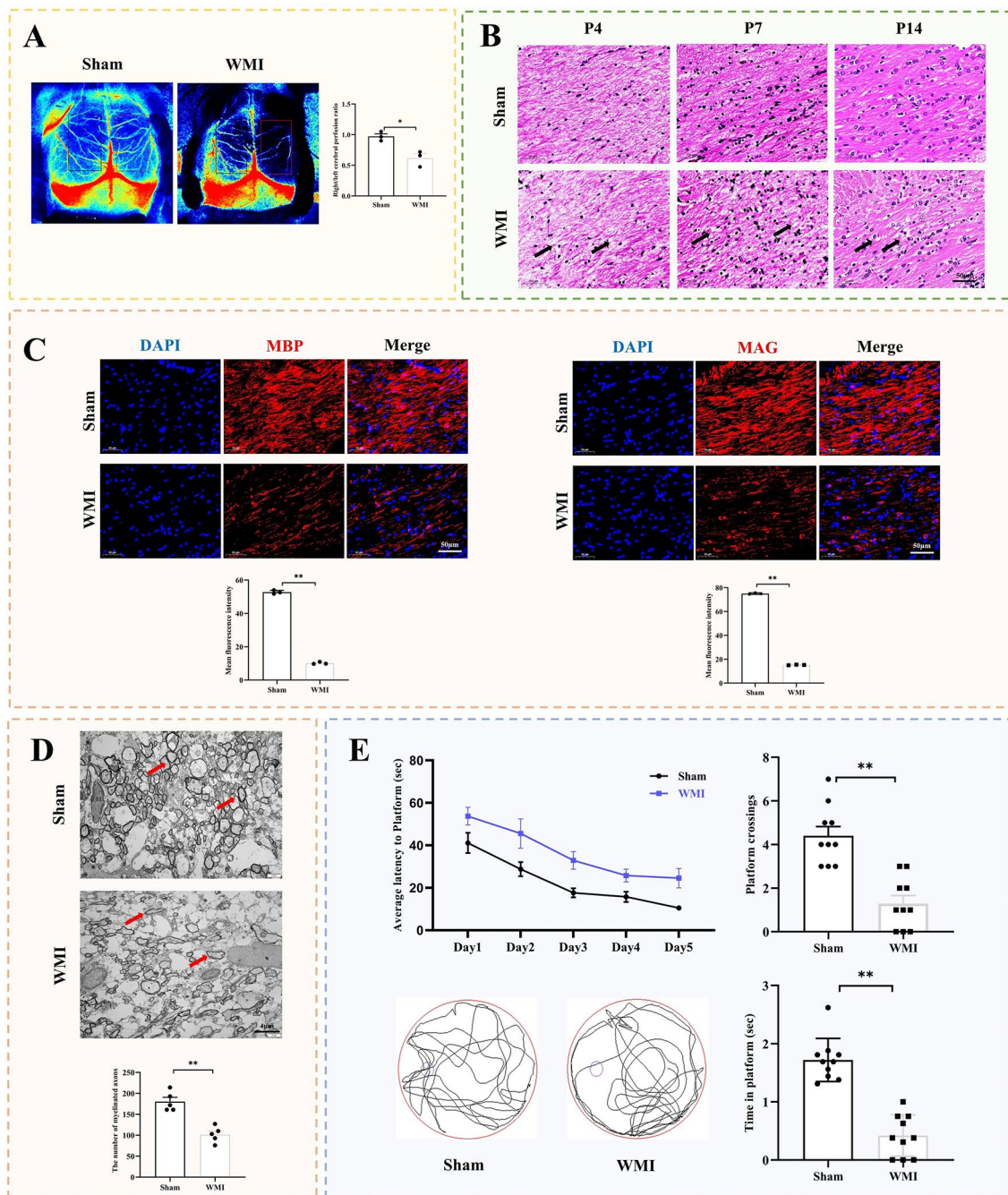


Fig. 2 Hypoxic ischemia-induced WMI in neonatal rats. **(A)** The laser speckle imaging system to evaluate the cerebral blood flow ($n=3$ per group). The right cerebral blood flow ratio within the region of interest in the WMI group was significantly decreased. **(B)** H&E staining to evaluate the histopathologic damage in the corpus callosum area at P4, P7, and P14 ($n=3$ per group). In the WMI group, the white matter tissue appeared swollen and broken, exhibiting a disordered arrangement, loose structure, and widened gaps. **(C)** Representative immunofluorescence images of MBP (red) or MAG (red) staining of mature oligodendrocytes at P14. Nuclei were stained with DAPI (blue) ($n=3$ per group). The mean fluorescence intensities of MBP and MAG in the white matter in the WMI group decreased. **(D)** Detection of the number of myelin sheath via electron microscopy at P14 ($n=3$ per group) showed a reduction in myelin content in the WMI group accompanied by irregular morphology. **(E)** Morris water maze experiment performed to observe behavioral performance of rats at P28 ($n=10$ per group). In the WMI group, the escape latency increased, whereas the frequency of platform crossings and average residence time in the platform area decreased. Data are presented as mean \pm standard deviation. * $p < 0.05$, ** $p < 0.01$. Sham, sham-operated group; WMI, white matter injury group; P, postnatal day; DAPI, 4',6-diamidino-2-phenylindole; MBP, myelin basic protein; MAG, myelin-associated glycoprotein

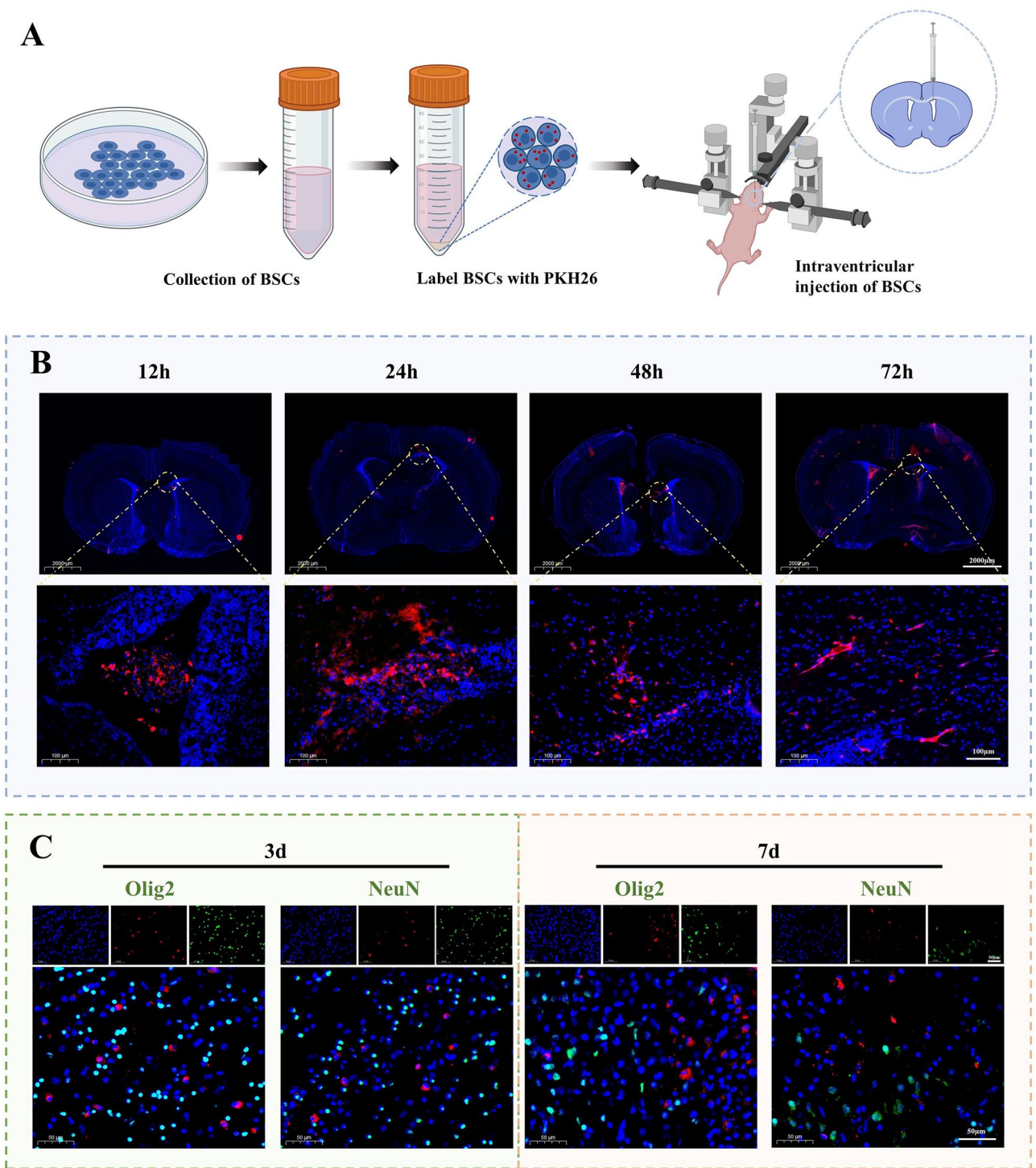


Fig. 3 Migration and differentiation of breastmilk stem cells (BSCs) after injection. **(A)** Schematic of the intraventricular injection of BSCs. **(B)** Immunofluorescence of PKH26 (red) to observe the migration of BSCs after injection. At 12 h post-injection, concentrated red fluorescence was observed in the lateral ventricle, whereas from 24 to 72 h post-injection, a scattered red fluorescence distribution was noted in the corpus callosum region on the injured side ($n=5$ per group). **(C)** Immunofluorescence performed to determine whether PKH26 (red) was co-stained with NeuN (green) and Olig2 (green) showed the differentiation of BSCs 3 and 7 days after injection. No co-staining cells of PKH26 with Olig2 or NeuN were observed ($n=5$ per group). BSCs, breastmilk stem cells

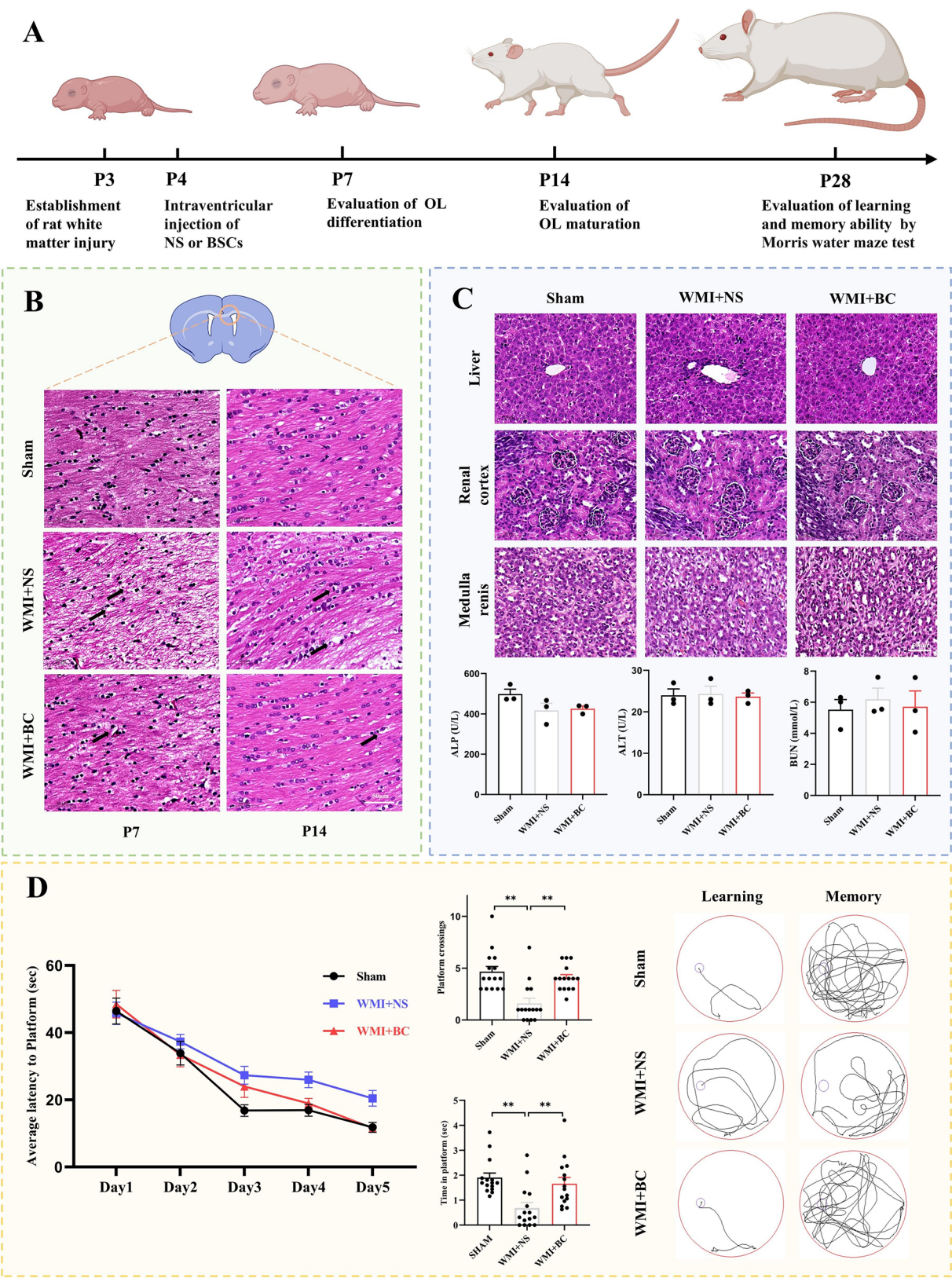


Fig. 4 (See legend on next page.)

(See figure on previous page.)

Fig. 4 Therapeutic effects of BSCs on WMI in newborn rats. **(A)** Schematic of the establishment of the WMI model, treatment, and evaluation timeline. **(B)** H&E staining to evaluate the histopathologic damage in the corpus callosum area at P7 and P14 ($n=5$ per group). The WMI+BC group showed significantly improved pathological changes in the white matter area of the injured side in newborn rats, leading to reduced swelling and breakage of nerve cells. **(C)** Hepatorenal function and hepatorenal H&E staining performed to determine safety of BSC treatment ($n=5$ per group). No significant differences in liver and kidney functions were observed. **(D)** Morris water maze experiment performed to observe the behavioral performance of rats at P28 ($n=15$ per group) showed that the WMI+BC group exhibited a shorter latency escape time and increased number and times of platform crossing. Data are presented as mean \pm standard deviation. * $p < 0.05$, ** $p < 0.01$. P, postnatal day; Sham, sham-operated group; WMI+BC, white matter injury with breastmilk cell group; WMI+NS, white matter injury with normal saline group; BSC, breastmilk stem cells; OL, oligodendrocytes; ALP, alkaline phosphatase; ALT, alanine transaminase; BUN, blood urea nitrogen

Related mechanisms of BSC treatment for WMI

Principal components analysis (PCA) was used to observe the overall distribution trend among all sample groups by reducing dimensionality to yield more reliable data analysis results. Our PCA results revealed distinct areas in two-dimensional space where samples from the sham, WMI+NS, and WMI+BC groups were distributed, with samples from the same group exhibiting a concentrated distribution (Fig. 6A). The results of the cytokine antibody assay identified 10 differentially expressed proteins among the WMI+BC, WMI+NS, and sham groups (Fig. 6B). Among them, five proteins showed potential relevance to OL differentiation and maturation, including CX3CL1 (fractalkine), B7-2, MCP-1, and eotaxin (Fig. 6C). In the Gene Ontology biological process analysis, the top five biological processes identified were response to interleukin 1, response to interferon- γ , regulation of T-cell activation, regulation of lymphocyte activation, and regulation of intraleukocytic adhesion (Fig. 6D). The first two processes may be associated with inflammation. Therefore, the next step was to study the inflammatory response during OL differentiation and maturation.

Western blot analysis revealed reduced expression levels of fractalkine and CX3CR1 in the WMI+BC group compared with that in the WMI+NS group (Fig. 6F and G). CX3CR1 distribution in the microglia was observed through immunofluorescence co-staining. Western blot analysis revealed a significant increase in the expression level of B7-2 in the WMI+NS group than in the sham group ($p < 0.01$). Conversely, compared with that in the WMI+NS group, the expression level of B7-2 in the WMI+BC group was significantly decreased ($p < 0.01$, Fig. 6E). Immunofluorescence analysis showed that the B7-2+/Iba1+ cell count decreased in the WMI+BC group ($p < 0.01$). Similarly, CD206+/Iba1+ cell count increased in the WMI+BC group ($p < 0.01$, Fig. 6H). qRT-PCR results demonstrated an increase in mRNA expression levels of proinflammatory factors (*Il1b*, *Il6*, *Ifng*, and *Tnfa*) in the WMI+NS group, whereas a decrease was observed in the WMI+BC group ($p < 0.01$). Conversely, the mRNA expression of anti-inflammatory factors (*Arg1* and *Tgfb*) decreased in the WMI+NS group and increased in the WMI+BC group ($p < 0.01$, Fig. 6J).

Discussion

According to estimates from the World Health Organization, approximately 15 million premature babies are born worldwide each year, constituting 11.1% of all newborns [9]. Despite significant improvements in perinatal care quality and preterm survival rates, many surviving preterm infants still experience neurodevelopmental impairments [10]. WMI is the most common form of brain damage in preterm infants, often leading to short- or long-term neurodevelopmental defects [11]. Early damage to the developing brain can affect multiple domains, including motor, cognitive, behavioral, visual, and auditory functions [12]. Hypoxic ischemia is a major mechanism of perinatal brain injury [13], primarily affecting the white matter in premature infants [14, 15]. Within the brain's white matter, OLs predominate and are more vulnerable to ischemia than other glial cells and even neurons in certain brain regions and developmental stages [16]. WMI incidence peaks between 23 and 32 weeks of gestation, a critical period for OL development, when pre-OLs are predominant and particularly vulnerable to hypoxia and inflammation [17]. The main pathological features of WMI in preterm infants are developmental arrest, decreased myelination of oligodendrocyte lineage, axon swelling or degeneration, and activation of microglia. The main mechanisms involved in the occurrence and development of WMI are ischemia, hypoxia and inflammation [18].

Breastmilk contains many bioactive components, including oligosaccharides, active proteins, exosomes, probiotics, cytokines, and various cells, significantly affecting infant immune regulation and development. Among these cells are stem cells, progenitor cells, white blood cells, macrophages, neutrophils, epithelial cells, monocytes, and lymphocytes. In 2007, *Nestin*-positive cells, identified as pluripotent stem cells, were first discovered in breastmilk [6]. Patki et al. found that BSCs exhibit mesenchymal stem cell properties and can differentiate into fat, cartilage, and bone cell lineages [7]. Hassiotou et al. found that BSCs express genes similar to those in embryonic stem cells and can differentiate into cells from all three embryonic layers (pancreas, cartilage, and neurons) [8].

Currently, owing to insufficient studies, the nature of BSCs remains controversial. In this study, flow cytometry

results demonstrated that the obtained BSCs expressed the mesenchymal stem cell positive markers CD29, CD166, CD73, CD105, CD44, and CD90 while also expressing the mesenchymal stem cell negative markers HLA-DR, CD79a, and CD45. Notably, the mesenchymal stem cell marker STRO-1 and the hematopoietic stem cell marker CD34 were not expressed, indicating distinctions from previously reported BSCs. Furthermore, flow cytometry and immunofluorescence results revealed the absence of the pluripotent stem cell markers *SOX2*, *Nanog*, *OCT4*, *SSEA4*, and *TRA-1-60*, suggesting divergence from BSCs possessing embryonic stem cell properties. Notably, the cultured BSCs expressed markers associated with nerve stem/progenitor cells such as *Vimentin*, *Nestin*, and *A2B5*, implying potential characteristics of nerve stem/progenitor cells. Although the properties of the obtained BSCs did not precisely align with those reported in previous studies, they exhibited properties of both mesenchymal and neural stem cells. Regarding the role of BSCs, Kaingade et al. found that BSCs can secrete vascular endothelial and hepatocyte growth factors in vitro [19]. Additionally, Borhani-Haghighi et al. found that intravaginal injection of the BSC culture supernatant reduced apoptosis and inflammatory responses at the injury site in rats with spinal cord injury, improving their sensory and motor conditions [20].

OLs undergo four distinct stages of maturation in both humans and rodents: oligodendrocyte precursor cell (OPCs), pre-OLs, immature OLs, and mature OLs [21]. OL precursor cells are highly proliferative, motile bipolar cells that express *A2B5*, *PDGF- α* receptors, and *NG2* [22]. OPCs migrate in the brain and will further differentiate into pre-OLs with multiple branches when they reach specific regions of the brain [23]. pre-OLs are characterized by the expression of *NG2* and *O4*. Then OLs will continue to differentiate into immature OLs and mature OLs with myelin generation ability. Mature OLs gradually myelinate and enclose axons to form myelin sheaths. Mature OLs express myelin proteins such as *MBP*, *MAG*, etc [24]. Studies have found that these immature cell types are more sensitive to prematurity-related injuries than mature oligodendrocytes [25]. Inflammation and hypoxia, two injuries that are clearly associated with preterm birth, are the two main causes of disrupted development of the OL lineage. In vitro experiments have shown that 90% of oligodendrocytes will die within 9 h after 30 min of oxygen-glucose deprivation [26]. Hypoxia also leads to alterations in the concentration of signaling proteins and nutrients that are critical for normal growth and OPC differentiation in the developing brain [27]. In animal models, a proliferative response occurs after OL depletion due to hypoxia or inflammation, generating new OPCs, but developmental arrest leads to

incomplete maturation of OL and impaired myelination [28]. In this study, BSC treatment significantly improved pathological changes in the white matter area on the injured side of newborn rats, thereby alleviating nerve cell swelling and breakage. OL differentiation and maturation improved after BSC treatment and myelin sheath numbers increased. The learning and memory abilities of WMI rats also improved.

Fractalkine, also known as *CX3CL1*, is the sole member of the *CX3C* chemokine family. Within the central nervous system, fractalkine is secreted by neurons and predominantly expressed in mature neurons of the hippocampus, striatum, and cortex [29]. Fractalkine binds to its receptor *CX3CR1*, primarily expressed in microglia and associated with microglial chemotaxis, neurotoxicity, and activation [30]. The effects of fractalkine/*CX3CR1* on OLs have been studied using cellular and animal models. For example, oxygen and glucose deprivation (OGD) or OGD + fractalkine significantly increased microglia expression in vitro, decreased OL proliferation, increased apoptosis, and reduced *PLP* expression [31].

Additionally, Du et al. found that the downregulation of *CX3CR1* reduced serum *IL-1 β* , *IL-6*, and *TNF- α* levels and inhibited microglial activation, thus significantly reversing depression-like behavior and cognitive impairment in mice with global cerebral ischemia and promoting OL precursor cell differentiation and maturation into mature OLs [32]. Ischemia may promote fractalkine production and release, increasing the number of activated microglia and production of harmful cytokines in the microglia, ultimately contributing to OL injury. The role of fractalkine/*CX3CR1* in ischemic brain injury is likely more complex than currently understood, and the above contradictory results may be caused by variations in disease environments, experimental models, injury severity, and activation times of specific environmental signals [33]. In this study, fractalkine and *CX3CR1* were upregulated following WMI but downregulated after BSC treatment. Combined with previous literature, BSCs may reduce the activation of proinflammatory significantly lower compared with glia through fractalkine/*CX3CR1*, reduce the levels of inflammatory factors, improve neuroinflammation, and promote OL differentiation and maturation. However, the role of fractalkine/*CX3CR1* remains debated, and further investigation is required to determine whether BSCs regulate microglia through fractalkine/*CX3CR1*.

Microglia are immune cells within the central nervous system, constituting approximately 5–12% of total nerve cells in the mouse brain and approximately 0.5–16% in the human brain [34]. Microglia can not only activate neuroinflammatory pathways leading to progressive neurodegeneration, but also play a neuroprotective role by down-regulating inflammation and promoting

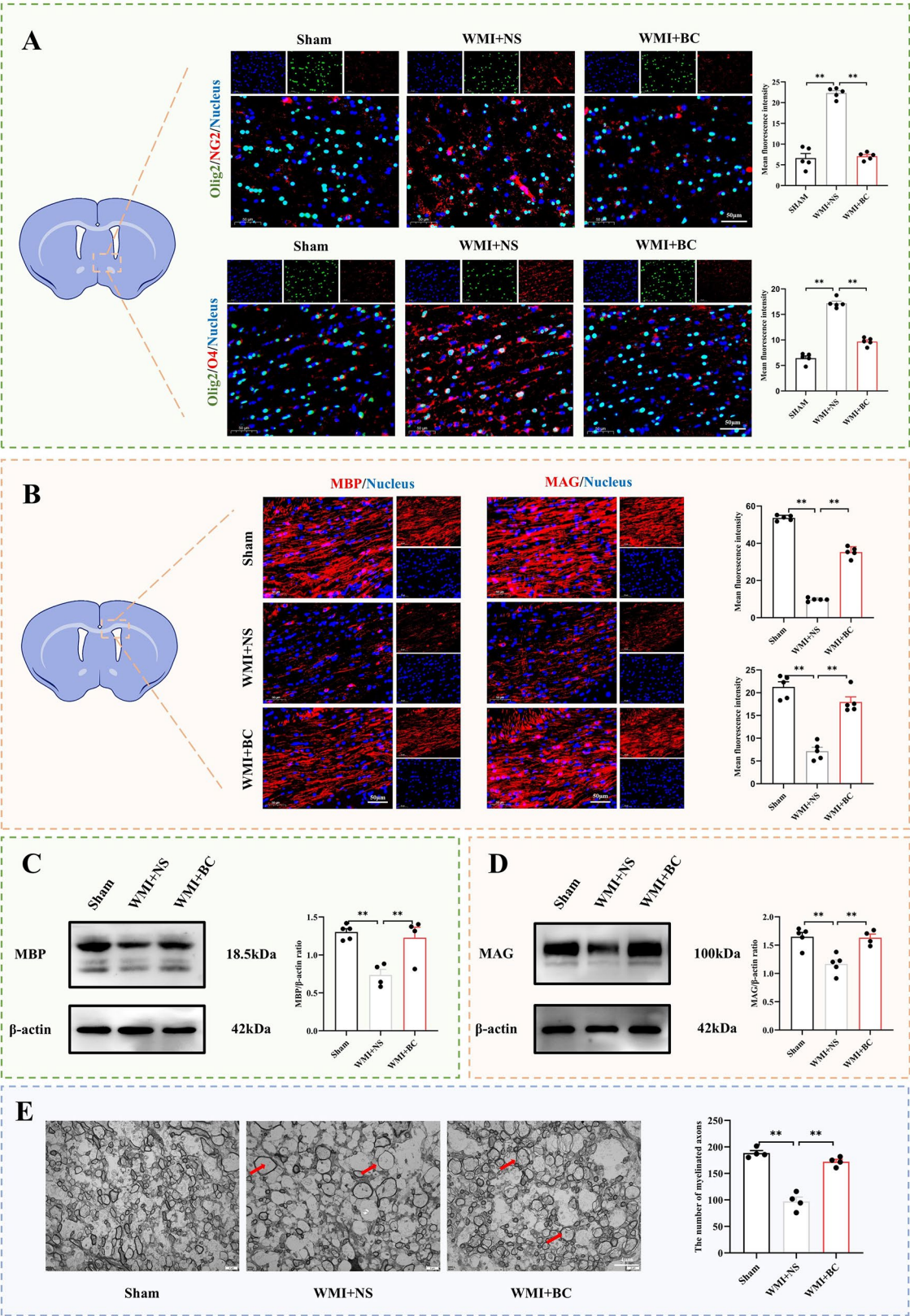


Fig. 5 (See legend on next page.)

(See figure on previous page.)

Fig. 5 BSCs improved the differentiation, maturation, and myelination of OLs. **(A)** Representative immunofluorescence images of O4 (red) or NG2 (red) and Olig2 (green) staining of mature OLs at P7 in the CC area. Nuclei were stained with DAPI (blue) ($n=5$ per group). Compared with the WMI + NS group, the WMI + BC group revealed a decreased expression of the pre-OL markers NG2 and O4 in the CC area. **(B)** Representative immunofluorescence images of MBP (red) or MAG (red) staining of mature OLs at P14 in the CC area. Nuclei were stained with DAPI (blue) ($n=5$ per group). Compared with the WMI + NS group, the WMI + BC group revealed an increased expression of the mature OL markers MBP and MAG in the CC area. **(C)** Western blotting and corresponding quantification to examine the expression of MBP at P14 ($n=5$ per group). Full-length blots are presented in Supplementary Fig. 3. Compared with the WMI + NS group, the WMI + BC group revealed an increased expression of the mature OL markers MBP. **(D)** Western blotting and corresponding quantification to examine the expression of MAG at P14 ($n=5$ per group). Full-length blots are presented in Supplementary Fig. 4. Compared with the WMI + NS group, the WMI + BC group revealed an increased expression of the mature OL markers MAG. **(E)** Detection of the number of myelin sheath via electron microscopy at P14 ($n=4$ per group). The WMI + BC group exhibited more myelination with a more regular pattern than the WMI + NS group. Data are presented as mean \pm standard deviation. * $p < 0.05$, ** $p < 0.01$. Sham, sham-operated group; WMI + BC, white matter injury with breastmilk cell group; WMI + NS, white matter injury with normal saline group; DAPI, 4',6-diamidino-2-phenylindole; MBP, myelin basic protein; MAG, myelin-associated glycoprotein; BSC, breastmilk stem cells; CC, corpus callosum

neuronal repair. Their activation is heterogeneous and has traditionally been classified as either neurotoxic (pro-inflammatory M1 microglia) or neuroprotective (anti-inflammatory M2 microglia). Proinflammatory microglia can produce and release proinflammatory factors, such as interleukin IL-1 β , IL-6, IFN- γ , TNF- α , and MCP-1, which can be detected and quantified by measuring the expression of cell surface markers, such as CD86, CD16, CD11b, and CD32 [35]. On the contrary, anti-inflammatory microglia can play a neuroprotective role by secreting anti-inflammatory mediators, such as IGF-1, IL-4, IL-10, etc [36], to reduce inflammatory response and repair damaged tissues, and M2 microglia express cell surface markers, such as CD206, CD163 and Arg1 [37].

Many studies have demonstrated the presence of activated microglia in various brain regions during different phases of ischemia [38, 39].

In vivo studies have found that activated microglia are enriched at the ischemic site 3–7 d after stroke [40]. Activated microglia could be detected in the border zone of ischemic lesions 30 min after permanent middle cerebral artery occlusion [30]. M2 microglia could be detected in the peri-infarct zone one day after occlusion. However, M1 microglia gradually increased from the 3rd day to the 14th day after injury [41]. After neonatal hypoxic-ischemic brain damage, the number of M2 microglia decreases with the increase of M1 microglia [42]. Study have suggested that the reciprocity of M1/M2 microglia appears to be a complicated time-dependent continuum following neonatal hypoxic-ischemic brain injury, with an early M1 response and delayed M2 response [43]. A single-cell transcriptomic analysis of microglia has shown that some cells simultaneously express both M1 and M2 markers, but lack consistency in M2 marker expression [44].

Throughout brain development, microglia directly and indirectly regulate OL function [45, 46]. Microglial activation significantly contributes to pre-OL and OL injuries in ischemic WMI. Following hypoxia, activated M1 microglia cells produce excess inflammatory factors, such as TNF- α and IL-1 β , glutamic acid, nitric oxide, and reactive oxygen species [47]. High levels of proinflammatory

cytokines such as IL-1 β , TNF- α , and IL-2 have been detected in the brains of patients with diffuse WMI [48]. Although activated microglia are harmful to OL progenitor cells, they promote the survival of mature OLs [49]. Preterm infants possess numerous OL precursor cells in their brain white matter, rendering them extremely vulnerable to the influence of proinflammatory factors. Both in vivo and in vitro experimental models have demonstrated the negative effects of these factors on OL progenitor proliferation, differentiation, and survival [50]. However, studies have also highlighted the beneficial effects of M2 microglia on OL proliferation and differentiation. M2 microglia cells produce and release anti-inflammatory cytokines. In vitro studies have shown that conditioned medium from LPS-induced M1 microglia increases OL death following OGD, whereas conditioned medium from IL-4-induced M2 microglia decreases OL apoptosis [51]. Treatment aimed at reducing M1 microglia and increasing M2 microglia in newborn mice has been shown to improve demyelination [52] and alleviate cognitive-behavioral deficits [53]. In this study, our findings suggest an augmented neuroinflammatory response, which could adversely affect OL differentiation, maturation, and myelination. BSCs reduce proinflammatory cytokine secretion while increasing anti-inflammatory cytokines, thereby alleviating inflammation in the brain's white matter region. This, in turn, promoted OL differentiation and maturation, ultimately improving white matter damage.

The potential of BSCs to differentiate into nerve cells post-injection and play a substitutive role requires further investigation. Previous studies have suggested that BSCs can differentiate into neurons and OLs in vitro [54]. Other studies found that green fluorescent protein-positive cells were distributed in the brain and blood after newborn mice were breastfed by transgenic female mice expressing green fluorescent protein, suggesting that BSCs differentiated in the brain [55]. However, our study's results indicate that BSCs failed to differentiate into OLs or neurons in the rat brain 3 and 7 days post-injection. On the question of long-term survival and differentiation of BSCs, owing to the limited amount of

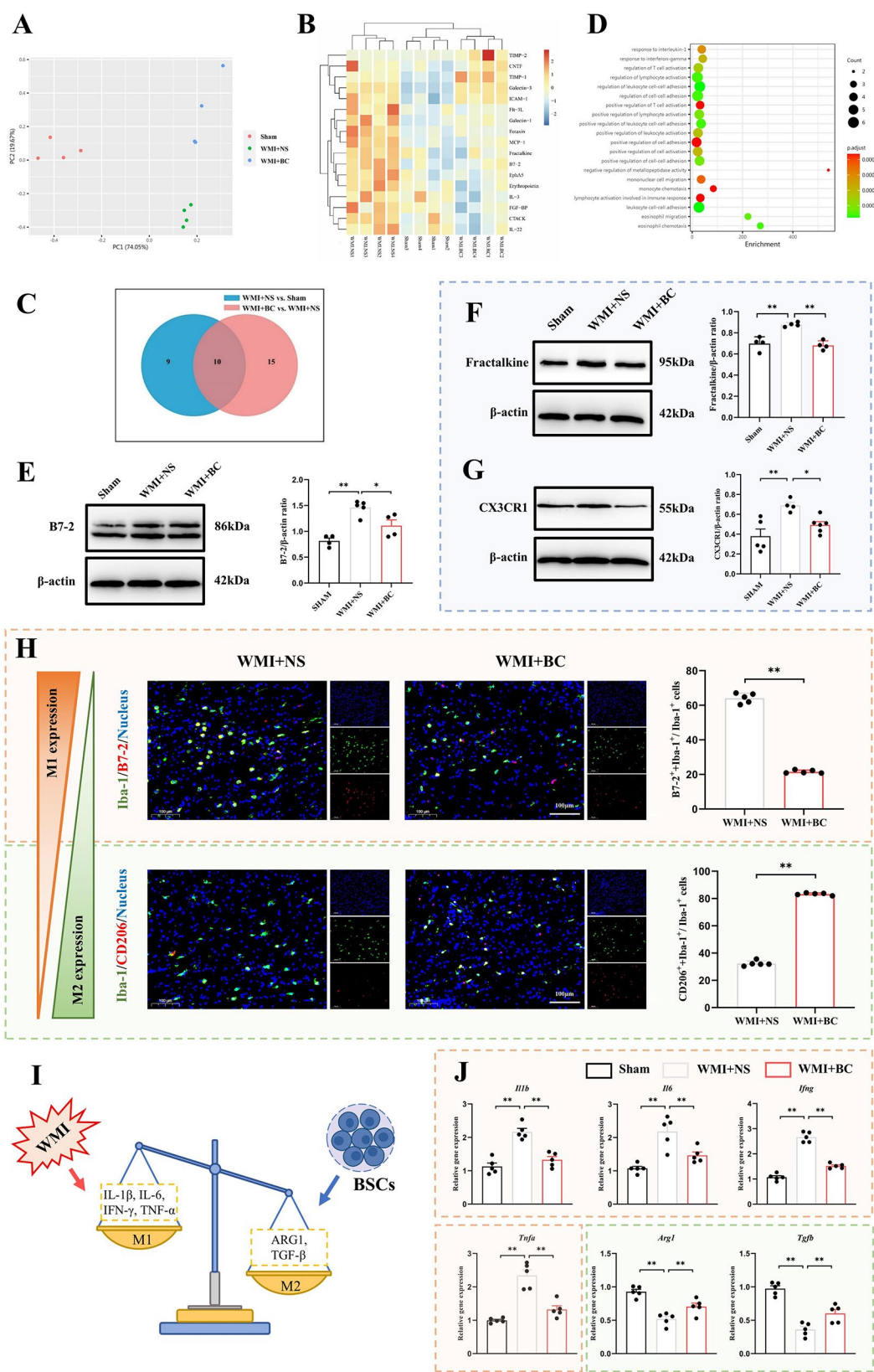


Fig. 6 (See legend on next page.)

(See figure on previous page.)

Fig. 6 Related mechanisms of BSC treatment for WMI. **(A)** Principal components analysis of brain samples of protein chip in different groups ($n=4$ per group). The samples from the same group exhibited a concentrated distribution. **(B)** Seventeen differential proteins in any two groups were screened in the heat map by the protein chip. **(C)** Venn diagram of differential proteins among the WMI + BC, WMI + NS, and sham groups. The results of the cytokine antibody assay identified 10 differentially expressed proteins among the three groups. **(D)** In the Gene Ontology biological process analysis, the top five biological processes identified were response to interleukin 1, response to interferon- γ , regulation of T-cell activation, regulation of lymphocyte activation, and regulation of intraleukocytic adhesion. **(E)** Validation of the expression of the differential protein B7-2 at P7 via western blotting. Full-length blots are presented in Supplementary Fig. 5. Compared with that in the WMI + NS group, the expression level of B7-2 in the WMI + BC group was significantly decreased ($n=5$ per group). **(F)** Validation of the expression of the differential protein fractalkine at P7 via western blotting ($n=5$ per group). Full-length blots are presented in Supplementary Fig. 6. **(G)** Western blotting and corresponding quantification to examine the expression of receptor protein CX3CR1 for the differential protein fractalkine at P7 ($n=5$ per group). Full-length blots are presented in Supplementary Fig. 7. Western blot analysis revealed reduced expression levels of fractalkine and CX3CR1 in the WMI + BC group compared with that in the WMI + NS group. **(H)** Representative immunofluorescence images of B7-2 (red) and CD206 (red) staining of microglia (marked by Iba-1 with green fluorescence) at P7 in the corpus callosum area ($n=5$ per group). The B7-2+/Iba1+ cell count decreased in the WMI + BC group, whereas CD206+/Iba1+ cell count increased in the WMI + BC group. **(I)** Schematic of the possible effect of BSCs in microglia polarization regulation. **(J)** The expressions of IL-1 β , IL-6, IFN- γ , TNF- α , ARG1, and TGF- β mRNAs measured at P7 by qRT-PCR ($n=5$ per group). Compared with that in the WMI + NS group, the expression level of IL-1 β , IL-6, IFN- γ , and TNF- α in the WMI + BC group was significantly decreased, whereas the expression levels of ARG1 and TGF- β were significantly increased. Data are presented as mean \pm standard deviation. * $p < 0.05$, ** $p < 0.01$. Sham, sham-operated group; WMI + BC, white matter injury with breastmilk cell group; WMI + NS, white matter injury with normal saline group; BSC, breastmilk stem cells

colostrum collected, we were not able to perform related experiments at additional time points. We found in our pilot study that PKH26 labeling could not be traced in rat brain at P28. In our study, we suggest that the therapeutic effects of BSCs may be related to their early anti-inflammatory effect, which may affect the long-term differentiation and maturation of OLs through the repair of inflammation through paracrine action. There are few studies on the in vivo differentiation of BSCs post-injection, and the possible underlying mechanism requires further exploration.

Our study innovatively obtained BSCs with different characteristics from previous literature, which led to the filing of an invention patent [56]. These BSCs expressed certain mesenchymal and neural stem cell markers but lacked the expression of embryonic stem cell markers. They differed from mesenchymal or embryonic stem cell-like cells obtained from breastmilk in previous studies, displaying some neural stem cell markers. Despite these advancements, our study has some limitations. For example, the characteristics of breast milk stem cells is not well understood. In vitro, it is not clear what differentiation direction and differentiation potential the cells derived from human milk have. More experiments and time are needed to clarify the characteristics of breast milk stem cells due to the limitation of breast milk collection and cell culture. Also, the underlying mechanism of fractalkine/CX3CR1 in ischemic hypoxia-related brain injury requires further investigation, and the relationship between fractalkine/CX3CR1 and microglial regulation remains unclear. Additionally, multiple mechanisms may underlie stem cell therapy, warranting further studies on other possible mechanisms, such as their influence on angiogenesis and apoptosis.

Conclusions

Our findings suggest that BSCs can improve the maturation of OLs following WMI in newborn rats. The mechanisms may be attributed to the reduced proinflammatory microglia cells and factors as well as the increased anti-inflammatory microglia cells and factors due to the downregulation of fractalkine/ CX3CR1.

Abbreviations

ALP	Alkaline phosphatase
ALT	Alanine transaminase
Arg1	Arginase 1
B7-2	B-lymphocyte antigen
BSCs	Breastmilk stem cells
BUN	Blood urea nitrogen
CC	Corpus callosum
CX3CL1	Chemokine C-X3-C motif ligand 1
CX3CR1	Chemokine C-X3-C motif receptor 1
DAPI	4',6-diamidino-2-phenylindole
H&E	Hematoxylin and eosin
HLA-DR	Human leukocyte antigen-DR
Iba1	Ionized calcium binding adapter molecule 1
Ifng	Interferon- γ
Ig	Immunoglobulin
Il1b	Interleukin-1 β
Il6	Interleukin-6
MAG	Myelin Associated Glycoprotein
MBP	Myelin Basic Protein
MCP-1	Monocyte chemoattractant protein-1
MWM	Morris water maze
NeuN	Neuronal Nuclei
NG2	Neuron-glia Antigen2
NS	Normal saline
O4	Oligodendrocyte Marker 4
OCT4	Octamer Binding Transcription Factor 4
OGD	Oxygen and glucose deprivation
OL	Oligodendrocyte
Olig2	Oligodendrocyte transcription factor 2
OPCs	Oligodendrocyte precursor cells
P	Postnatal day
PBS	Phosphate-buffered saline
PCA	Principal components analysis
PLP	Myelin proteolipid protein
qRT-PCR	Quantitative Real-time Polymerase Chain Reaction
SD	Sprague-Dawley
SOX2	Sex determining region Y-box 2
SSEA4	Stage-specific embryonic antigen-4

Tgfb Transforming growth factorβ
Tnfa Tumor necrosis factorα
TRA-1-60 Tumor-related antigen-1-60
WMI White matter injury

Supplementary Information

The online version contains supplementary material available at <https://doi.org/10.1186/s13287-025-04257-x>.

Supplementary Material 1
Supplementary Material 2
Supplementary Material 3
Supplementary Material 4
Supplementary Material 5
Supplementary Material 6
Supplementary Material 7
Supplementary Material 8

Acknowledgements

Not applicable.

Author contributions

MZ and HW contributed to experimental studies, data analysis and manuscript preparation. YH, WL, HC and XZ contributed to statistical analysis. QC, CY, ML and BZ contributed to experimental studies. JT and DM contributed to design the conception and manuscript editing and manuscript review. We declare that we have not use AI-generated work in this manuscript.

Funding

This work was supported by the National Natural Science Foundation of China [82171710, 82271749]; the grants from the Science and Technology Bureau of Sichuan Province [2020YJ0236].

Data availability

The datasets used and analysed during the current study are available from the corresponding author on reasonable request. All additional files are included in the manuscript.

Declarations

Ethics approval and consent to participate

This study (Effects and mechanisms of breastmilk stem cells in the treatment of white matter injury in newborn rats) received approval from the Institutional Ethics Committee of West China Second Hospital, Sichuan University (No. 2020083) on 30 March 2020. The ethics approval included permission for (1) performing experiments on newborn rats and treating the newborn rats with human cells; (2) collection of human breast milk, isolation and culture of breastmilk cells with informed patient consent. The patients provided written informed consent for the use of samples.

Consent for publication

Not applicable.

Competing interests

The authors declare that they have no competing interests.

Author details

¹Department of Pediatrics, West China Second Hospital, Sichuan University, No. 20, Section 3, Renmin South Road, Chengdu 610041, China

²Key Laboratory of Birth Defects and Related Diseases of Women and Children, Sichuan University, Ministry of Education, No. 17, Section 3, Renmin South Road, Chengdu, Sichuan 610041, China

³Sichuan Cord Blood Bank, Chengdu 610037, China

Received: 19 September 2024 / Accepted: 27 February 2025

Published online: 07 March 2025

References

1. Pierrat V, Marchand-Martin L, Arnaud C, Kaminski M, Resche-Rigon M, Lebeaux C, et al. Neurodevelopmental outcome at 2 years for preterm children born at 22 to 34 weeks' gestation in France in 2011: EPIPAGE-2 cohort study. *BMJ*. 2017;358:j3448.
2. Lv H, Wang Q, Wu S, Yang L, Ren P, Yang Y, et al. Neonatal hypoxic ischemic encephalopathy-related biomarkers in serum and cerebrospinal fluid. *Clin Chim Acta*. 2015;450:282–97.
3. Silveira RC, Procianny RS. Hypothermia therapy for newborns with hypoxic ischemic encephalopathy. *J Pediatr (Rio J)*. 2015;91(6 Suppl 1):S78–83.
4. Nabetani M, Shintaku H, Hamazaki T. Future perspectives of cell therapy for neonatal hypoxic-ischemic encephalopathy. *Pediatr Res*. 2018;83(1–2):356–63.
5. Gila-Diaz A, Arribas SM, Algara A, Martin-Cabrejas MA, Lopez de Pablo AL, Saenz, de Pipaon M et al. A Review of Bioactive Factors in Human Breastmilk: A Focus on Prematurity. *Nutrients*. 2019;11(6).
6. Villadsen R, Fridriksdottir AJ, Ronnov-Jessen L, Gudjonsson T, Rank F, LaBarge MA, et al. Evidence for a stem cell hierarchy in the adult human breast. *J Cell Biol*. 2007;177(1):87–101.
7. Patki S, Kadam S, Chandra V, Bhone R. Human breast milk is a rich source of multipotent mesenchymal stem cells. *Hum Cell*. 2010;23(2):35–40.
8. Hassiotou F, Beltran A, Chetwynd E, Stuebe AM, Twigger AJ, Metzger P, et al. Breastmilk is a novel source of stem cells with multilineage differentiation potential. *Stem Cells*. 2012;30(10):2164–74.
9. Blencowe H, Cousens S, Chou D, Oestergaard M, Say L, Moller AB, et al. Born too soon: the global epidemiology of 15 million preterm births. *Reprod Health*. 2013;10(Suppl 1):S2.
10. He Y, Zhang Y, Li F, Shi Y. White matter injury in preterm infants: pathogenesis and potential therapy from the aspect of the Gut-Brain Axis. *Front Neurosci*. 2022;16:849372.
11. Back SA, Miller SP. Brain injury in premature neonates: A primary cerebral dysmaturation disorder? *Ann Neurol*. 2014;75(4):469–86.
12. Schneider J, Miller SP. Preterm brain injury: white matter injury. *Handb Clin Neurol*. 2019;162:155–72.
13. Graham EM, Ruis KA, Hartman AL, Northington FJ, Fox HE. A systematic review of the role of intrapartum hypoxia-ischemia in the causation of neonatal encephalopathy. *Am J Obstet Gynecol*. 2008;199(6):587–95.
14. Gopagondanahalli KR, Li J, Fahey MC, Hunt RW, Jenkin G, Miller SL, et al. Preterm Hypoxic-Ischemic encephalopathy. *Front Pediatr*. 2016;4:114.
15. Murray AL, Thompson DK, Pascoe L, Leemans A, Inder TE, Doyle LW, et al. White matter abnormalities and impaired attention abilities in children born very preterm. *NeuroImage*. 2016;124(Pt A):75–84.
16. Magaki SD, Williams CK, Vinters HV. Glial function (and dysfunction) in the normal & ischemic brain. *Neuropharmacology*. 2018;134(Pt B):218–25.
17. Liu XB, Shen Y, Plane JM, Deng W. Vulnerability of premyelinating oligodendrocytes to white-matter damage in neonatal brain injury. *Neurosci Bull*. 2013;29(2):229–38.
18. Guillot M, Miller SP. The dimensions of white matter injury in preterm neonates. *Semin Perinatol*. 2021;45(7):151469.
19. Kaingade PM, Somasundaram I, Nikam AB, Sarang SA, Patel JS. Assessment of growth factors secreted by human breastmilk mesenchymal stem cells. *Breastfeed Med*. 2016;11(1):26–31.
20. Borhani-Haghighi M, Navid S, Mohamadi Y. The therapeutic potential of conditioned medium from human breast milk stem cells in treating spinal cord injury. *Asian Spine J*. 2020;14(2):131–8.
21. Newville J, Jantzie LL, Cunningham LA. Embracing oligodendrocyte diversity in the context of perinatal injury. *Neural Regen Res*. 2017;12(10):1575–85.
22. Domingues HS, Portugal CC, Socodato R, Relvas JB. Oligodendrocyte, astrocyte, and microglia crosstalk in Myelin development, damage, and repair. *Front Cell Dev Biol*. 2016;4:71.
23. Favrais G, Bokobza C, Saliba E, Chalon S, Gressens P. Alteration of the oligodendrocyte lineage varies according to the systemic inflammatory stimulus in animal models that mimic the encephalopathy of prematurity. *Front Physiol*. 2022;13:881674.
24. van Tilborg E, de Theije CGM, van Hal M, Wagenaar N, de Vries LS, Benders MJ, et al. Origin and dynamics of oligodendrocytes in the developing brain: implications for perinatal white matter injury. *Glia*. 2018;66(2):221–38.

25. Deng W. Neurobiology of injury to the developing brain. *Nat Rev Neurol*. 2010;6(6):328–36.
26. Tekkok SB, Goldberg MP. Ampa/kainate receptor activation mediates hypoxic oligodendrocyte death and axonal injury in cerebral white matter. *J Neurosci*. 2001;21(12):4237–48.
27. Huang J, Zhang L, Qu Y, Zhou Y, Zhu J, Li Y, et al. Histone acetylation of oligodendrocytes protects against white matter injury induced by inflammation and hypoxia-ischemia through activation of BDNF-TrkB signaling pathway in neonatal rats. *Brain Res*. 2018;1688:33–46.
28. Zhao SC, Ma LS, Chu ZH, Xu H, Wu WQ, Liu F. Regulation of microglial activation in stroke. *Acta Pharmacol Sin*. 2017;38(4):445–58.
29. Subbarayan MS, Joly-Amado A, Bickford PC, Nash KR. CX3CL1/CX3CR1 signaling targets for the treatment of neurodegenerative diseases. *Pharmacol Ther*. 2022;231:107989.
30. Qin C, Zhou LQ, Ma XT, Hu ZW, Yang S, Chen M, et al. Dual functions of microglia in ischemic stroke. *Neurosci Bull*. 2019;35(5):921–33.
31. Wu XM, Liu Y, Qian ZM, Luo QQ, Ke Y. CX3CL1/CX3CR1 Axis plays a key role in Ischemia-Induced oligodendrocyte injury via p38MAPK signaling pathway. *Mol Neurobiol*. 2016;53(6):4010–8.
32. Du B, Liang M, Zheng H, Fan C, Zhang H, Lu X, et al. Anti-mouse CX3CR1 antibody alleviates cognitive impairment, neuronal loss and Myelin deficits in an animal model of brain ischemia. *Neuroscience*. 2020;438:169–81.
33. Pawelec P, Ziemka-Nalecz M, Sypecka J, Zalewska T. The impact of the CX3CL1/CX3CR1 Axis in neurological disorders. *Cells*. 2020;9(10).
34. Lloyd AF, Davies CL, Miron VE. Microglia: origins, homeostasis, and roles in Myelin repair. *Curr Opin Neurobiol*. 2017;47:113–20.
35. Sen MK, Mahns DA, Coorssen JR, Shortland PJ. The roles of microglia and astrocytes in phagocytosis and myelination: insights from the Cuprizone model of multiple sclerosis. *Glia*. 2022;70(7):1215–50.
36. Contino M, Capparelli E, Colabufo NA, Bush AI, Editorial. The CB2 cannabinoid system: A new strategy in neurodegenerative disorder and neuroinflammation. *Front Neurosci*. 2017;11:196.
37. Tang Y, Le W. Differential roles of M1 and M2 microglia in neurodegenerative diseases. *Mol Neurobiol*. 2016;53(2):1181–94.
38. Gorlamandala N, Parmar J, Craig AJ, Power JM, Moorhouse AJ, Krishnan AV, et al. Focal ischaemic infarcts expand faster in cerebellar cortex than cerebral cortex in a mouse photothrombotic stroke model. *Transl Stroke Res*. 2018;9(6):643–53.
39. Hu X, Li P, Guo Y, Wang H, Leak RK, Chen S, et al. Microglia/macrophage polarization dynamics reveal novel mechanism of injury expansion after focal cerebral ischemia. *Stroke*. 2012;43(11):3063–70.
40. Perego C, Fumagalli S, De Simoni MG. Temporal pattern of expression and colocalization of microglia/macrophage phenotype markers following brain ischemic injury in mice. *J Neuroinflammation*. 2011;8:174.
41. Ma Y, Wang J, Wang Y, Yang GY. The biphasic function of microglia in ischemic stroke. *Prog Neurobiol*. 2017;157:247–72.
42. Jaworska J, Ziemka-Nalecz M, Sypecka J, Zalewska T. The potential neuroprotective role of a histone deacetylase inhibitor, sodium butyrate, after neonatal hypoxia-ischemia. *J Neuroinflammation*. 2017;14(1):34.
43. Hellstrom Erkenstam N, Smith PL, Fleiss B, Nair S, Svedin P, Wang W, et al. Temporal characterization of microglia/macrophage phenotypes in a mouse model of neonatal Hypoxic-Ischemic brain injury. *Front Cell Neurosci*. 2016;10:286.
44. Shao R, Sun D, Hu Y, Cui D. White matter injury in the neonatal hypoxic-ischemic brain and potential therapies targeting microglia. *J Neurosci Res*. 2021;99(4):991–1008.
45. Greenhalgh AD, David S, Bennett FC. Immune cell regulation of glia during CNS injury and disease. *Nat Rev Neurosci*. 2020;21(3):139–52.
46. McNamara NB, Miron VE. Microglia in developing white matter and perinatal brain injury. *Neurosci Lett*. 2020;714:134539.
47. Kaur C, Rathnasamy G, Ling EA. Roles of activated microglia in hypoxia induced neuroinflammation in the developing brain and the retina. *J Neuro-immune Pharmacol*. 2013;8(1):66–78.
48. van Tilborg E, Heijnen CJ, Benders MJ, van Bel F, Fleiss B, Gressens P, et al. Impaired oligodendrocyte maturation in preterm infants: potential therapeutic targets. *Prog Neurobiol*. 2016;136:28–49.
49. Miller BA, Crum JM, Tovar CA, Ferguson AR, Bresnahan JC, Beattie MS. Developmental stage of oligodendrocytes determines their response to activated microglia in vitro. *J Neuroinflamm*. 2007;4:28.
50. Moxon-Emre I, Schlichter LC. Evolution of inflammation and white matter injury in a model of transient focal ischemia. *J Neuropathol Exp Neurol*. 2010;69(1):1–15.
51. Wang G, Zhang J, Hu X, Zhang L, Mao L, Jiang X, et al. Microglia/macrophage polarization dynamics in white matter after traumatic brain injury. *J Cereb Blood Flow Metabolism: Official J Int Soc Cereb Blood Flow Metabolism*. 2013;33(12):1864–74.
52. Fan C, Long R, You Y, Wang J, Yang X, Huang S, et al. A novel PADRE-Kv1.3 vaccine effectively induces therapeutic antibodies and ameliorates experimental autoimmune encephalomyelitis in rats. *Clin Immunol*. 2018;193:98–109.
53. Aryanpour R, Zibara K, Pasbakhsh P, Jame'i SB, Namjoo Z, Ghanbari A, et al. 17beta-Estradiol reduces demyelination in Cuprizone-fed mice by promoting M2 microglia Polarity and regulating NLRP3 inflammasome. *Neuroscience*. 2021;463:116–27.
54. Hosseini SM, Talaei-Khozani T, Sani M, Owringi B. Differentiation of human breast-milk stem cells to neural stem cells and neurons. *Neurol Res Int*. 2014;2014:807896.
55. Aydin MS, Yigit EN, Vatanaslar E, Erdogan E, Ozturk G. Transfer and integration of breast milk stem cells to the brain of suckling pups. *Sci Rep*. 2018;8(1):14289.
56. Yang C, Tang J, Chen Q, Luo M, Zhang M, Zhang B, Mu D. Cells or cell compositions derived from breastmilk and its preparation method: China. Patent ZL 2022 1 05544158. 2023-11-03.

Publisher's note

Springer Nature remains neutral with regard to jurisdictional claims in published maps and institutional affiliations.